Combined use of field observations and SAR interferometry to study ice dynamics and mass balance in Dronning Maud Land, Antarctica

Reinhard Dietrich, Robert Metzig, Wilfried Korth & James Perlt

In the region of the Schirmacheroase (71°S, 12°E) various geodetic and glaciological research activities have been carried out in the last decade. Several times three geodetic-glaciological traverses were undertaken to study ice velocity, accumulation and ablation, and ice surface height changes. Repeated ground surveys show a significant decrease in surface heights by about 15 cm/y for a large blue-ice area. This paper presents the first interferometrically derived ice velocity field of the inland ice close to the Schirmacheroase. The interferometric analysis of the synthetic aperture radar (SAR) data is performed in combination with ground-based information. Since only ERS-1&2 tandem mission image couples are available for this region a digital elevation model (DEM) is used to remove the effect of topography. Ice velocities up to 100 m/y are proved interferometrically for this part of the inland ice.

R. Dietrich, R. Metzig, W. Korth & J. Perlt, Institut für Planetare Geodäsie, TU Dresden, D-01062 Germany.

Introduction

The determination of the mass balance of the Antarctic Ice Sheet is an important task of glaciological research in Antarctica (see e.g. Giovinetto et al. 1990). The ice mass flux across the grounding line or across other profiles delimiting an area of interest is one component of these investigations.

The application of airborne or spaceborne methods is the only promising way to cover entirely Antarctica. Repeat-pass synthetic aperture radar (SAR) interferometry can be applied to determine ice surface velocities as well as to detect the grounding line first demonstrated in (Goldstein et al. 1993). The following investigations in Dronning Maud Land were carried out to study the accuracy and the reliability of SAR interferometry as well as the possibilities of the combination of SAR data with ground truth information.

First we describe briefly the existing surface observations which serve as ground truth information. The next section focusses on the analysis of SAR interferometry data from the ERS-1&2 tandem mission. The possibilities of product improvement and validation by means of ground truth data are emphasized. Finally, we give an outlook on the further use of the generated velocity field, combined with ice thickness observations, to determine components of the ice mass balance.

Ground based observations

Since 1988, geodetic measurements have been carried out to determine glaciological parameters in the region, especially along three traverses crossing either the inland ice or the ice shelf. The results are coordinates and heights of points and profiles, ice velocities, deformation parameters, etc. An overview of these classical geodetic measurements, including the glaciological interpretation, is given by Korth & Dietrich (1996).

Along the two southward directed traverses special measurements for mass balance studies were carried out. The coordinates of the traverse points were determined by classical distance and direction measurements as well as by Global Positioning System (GPS) observations for the epoch 1995. Summarizing the error budget for all

Fig. 1. Corner reflector on bedrock.

epochs and for different measurements, this leads to a final relative error of the ice surface velocity of smaller than 5%. Traverse sections crossing a large area with blue-ice showed a significant decrease of surface heights of 15 ± 3.5 cm/y. This value corresponds to a mass loss of about 13 ± 3 cmWE/y (Korth, Perlt et al. 1996).

During the GeoMaud 1995/96 expedition four corner reflectors for SAR interferometry were set up (see Fig. 1) and observed by GPS. The coordinates of these points were determined within the frame of the Scientific Committee on Antarctic Research (SCAR) GPS network (Dietrich 1996). The locations of the corner reflectors are marked in Fig. 2.

A digital elevation model (DEM) was determined, using GPS surface heights, trigonometric levelling and airborne radio echo sounding. The accuracy of this DEM is about ±10 to 30 m (Korth, Dietrich et al. 1998).

Interferometric processing of ERS-1&2 SAR tandem data

In 1996, during the ERS-1&2 tandem mission, several consecutive passes of ERS-1&2 suitable for SAR interferometry were acquired covering

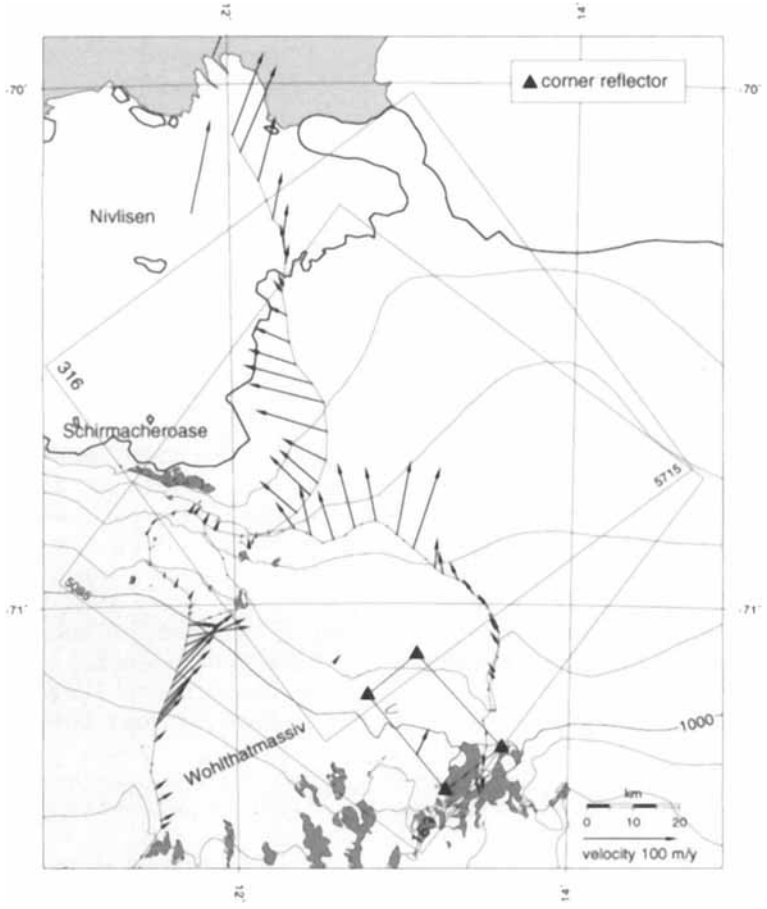

Fig. 2. Map of the working area. Selected SAR scenes and ice velocities from ground based measurements are included.

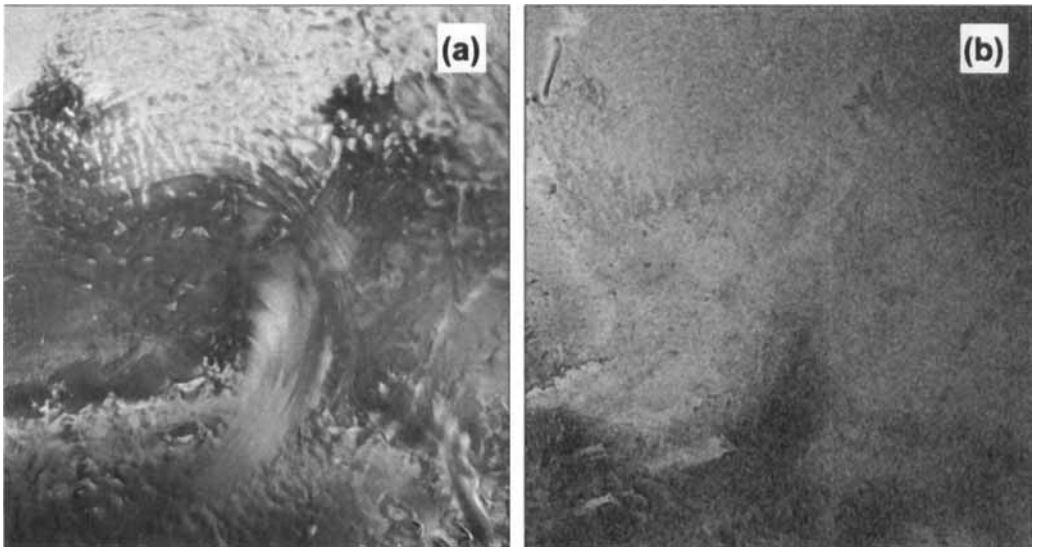

Fig. 3. (a) ERS-1 radar amplitude image of frame 5085 track 163 and (b) corresponding coherence image combining orbits 24700/ ERS-1 and 5027/ERS-2.

the region of the Schirmacheroase, Dronning Maud Land. All these passes were recorded at the Japanese Antarctic station Syowa. This study utilizes single look complex full scene (SLCI) images to compute amplitude and phase coherence images as well as interferograms. The main objective was to determine ice surface velocities. The short interferometric baselines during the time of acquisition were suitable for studying motion phenomena. Ascending and descending tracks were combined to derive velocity fields.

The interferograms presented in this paper were composed using descending orbits 24700 (ERS-1) and 5027 (ERS-2) as well as ascending orbits

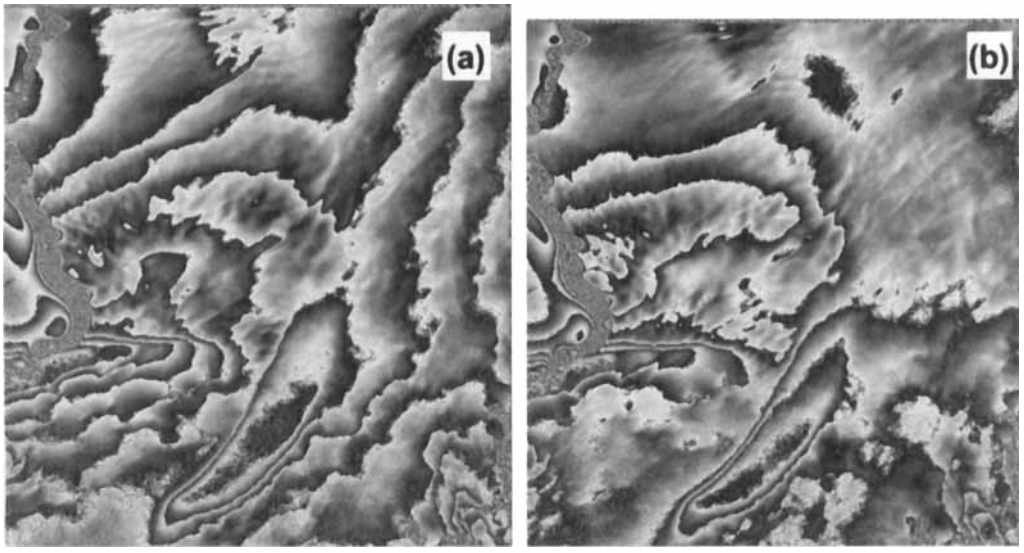

Fig. 4. Flattened interferograms of frame 5085 track 163 (B_n = 66.8 m): (a) without topographic correction; (b) with topographic correction.

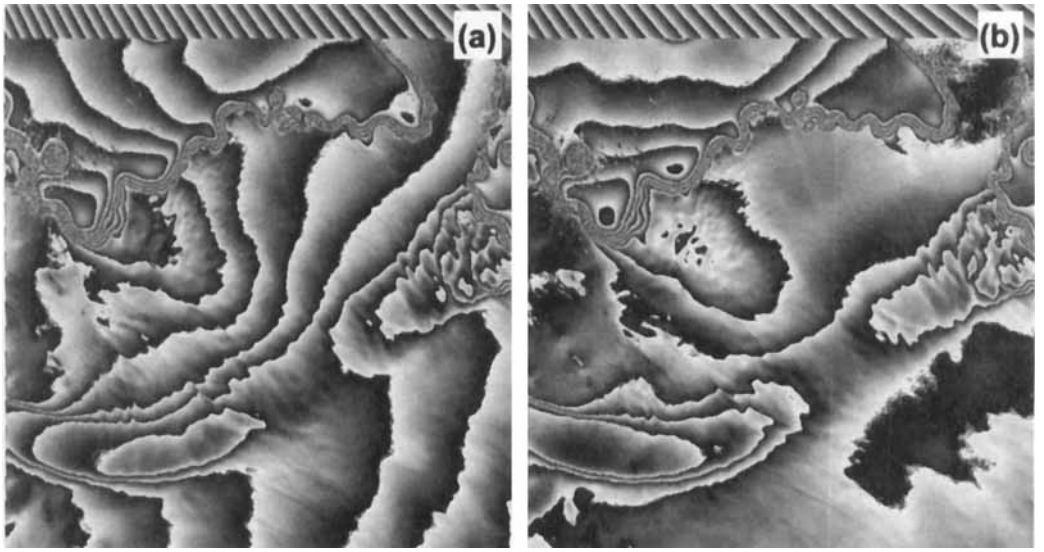

Fig. 5. Flattened and topography free interferograms of frame 5715 track 316. (a) Baseline calculation using precise ERS orbit products (B_n = 9.0 m). (b) Baseline estimation using four corner reflectors (B_n = 7.8 m).

25354 (ERS-1) and 5681 (ERS-2). To derive the horizontal ice velocity field, the overlapping frames 5085 (descending track) and 5715 (ascending track) shown in Fig. 1 are chosen.

The SLCIs were co-registered and then cross-correlated. The normalized correlation or phase coherence for frame 5085 is shown in Fig. 3. The coherence takes values between 0 (black, no correlation) and 1 (white, perfect temporal correlation). The corresponding amplitude image is also shown in Fig. 3.

Before velocity estimates can be made the interferometric phase fractions caused by the reference ellipsoid and the topography above this reference ellipsoid must be removed. Since only ERS-1&2 tandem mission image couples are available for this region, an independent digital elevation model (DEM) is used to remove the effect of topography (see also Massonnet et al. 1993). The DEM is derived from surface and airborne observations. For the longer interferometric baseline between orbits 24700 (ERS-1) and 5027 (ERS-2) the fringe pattern changes are significant with regard to topography (Fig. 4). The velocity error due to a DEM error is proportional to the baseline length and negligible for sufficient small baselines (Goldstein et al. 1993). Baseline errors due to the orbit inaccuracy affect in particular the phase ϕ_e of the reference ellipsoid used for flattening the interferogram. In Joughin et al. (1996) there is given an error model if using tie points to estimate the baseline. To estimate the maximum error due to the inaccuracy of precise ERS orbit products a slightly modified error model is used here. To derive the error, an expression for the phase ϕ_e containing the horizontal and vertical component of the baseline, B_y and B_z, respectively, is chosen, since the orbit accuracy is different for the across track and the radial component of the orbit vector. Because the velocity of any point can only be determined relatively to a point of known velocity the change of ϕ_e from near to far range is considered. Starting with

Table 1. Comparison of slant range displacement *dr* during consecutive passes of ERS-1&2 (orbit couple 25354 and 5681, Δt = 1 day, velocity reference point COR3). *gt* = ground truth; 1/2 = ERS-1&2.

Signal	dr_{gt} [m]	$dr_{1/2}$ [m]	dr_{gt}–$dr_{1/2}$ [m]
COR3	0.004	0.004	0.000
U9	0.001	0.002	−0.001
U10	0.005	0.005	0.000
U11	0.020	0.019	0.001
U13	0.060	0.057	0.002
U14	0.025	0.018	0.007
U15	0.013	0.013	0.000
U16	0.018	0.023	−0.005

$$\phi_e = -\frac{4\pi}{\lambda}\left[\sin(\theta_0 + \delta\theta_e)B_y - \cos(\theta_0 + \delta\theta_e)B_z + \frac{B^2}{2r}\right] \quad (1)$$

the change of ϕ_e from near to far range is given by

$$\begin{aligned}\Delta\phi_{e,far/near} = & -\frac{4\pi}{\lambda}\left[\sin(\theta_0 + \delta\theta_{e,far}) - \sin(\theta_0 + \delta\theta_{e,near})\right]B_y \\ & -\frac{4\pi}{\lambda}\left[\cos(\theta_0 + \delta\theta_{e,far}) - \cos(\theta_0 + \delta\theta_{e,near})\right]B_z \\ & -\frac{4\pi}{\lambda}\left[\frac{B^2}{2}\left(\frac{1}{r_{far}} - \frac{1}{r_{far}}\right)\right]. \end{aligned} \quad (2)$$

B indicates the baseline length and $\delta\theta_e$ is the angle between the reference-look direction and the intersection point of the slant range arc of radius r with the reference ellipsoid. A convenient choice is to let the nominal centre-look angle θ_0 define the reference-look direction (Joughin et al. 1996). The SAR wavelength is denoted as λ. Neglecting small non-linear terms, the maximum variance of $\Delta\phi_{e,far/near}$ is

$$\begin{aligned}\sigma^2_{\Delta\phi_{e,far/near},B} = & \left(\frac{4\pi}{\lambda}\right)^2\left([\sin(\theta_0 + \delta\theta_{e,far}) - \sin(\theta_0 + \delta\theta_{e,near})]\sqrt{2}\sigma_{s_y}\right)^2 \\ & + \left(\frac{4\pi}{\lambda}\right)^2\left([\cos(\theta_0 + \delta\theta_{e,far}) - \cos(\theta_0 + \delta\theta_{e,near})]\sqrt{2}\sigma_{s_z}\right)^2 \end{aligned}$$

$$\sigma_{B_y} \approx \sqrt{2}\sigma_{s_y}\ ,\ \sigma_{B_z} = \sqrt{2}\sigma_{s_z} \quad (3)$$

σ_{s_y} and σ_{s_z} denote the accuracy of the respective orbit vector in across track and radial direction. For the precise ERS orbit products the respective values are about 30–100 cm across track (Geudtner 1995) and about 8 cm (Gruber et al. 1996)/ 5 cm (Scharroo & Visser 1998) radial. If the vertical component of the ice velocity is neglected (a reasonable assumption for areas of slight surface slope) the maximum variance of the ice velocity due to the orbit inaccuracy can be expressed as

$$\begin{aligned}\sigma^2_{v_y,B} = & \frac{2}{(\Delta t \sin\eta)^2}\left([\sin(\theta_0 + \delta\theta_{e,far}) - \sin(\theta_0 + \delta\theta_{e,near})]\sigma_{s_y}\right)^2 \\ & + \frac{2}{(\Delta t \sin\eta)^2}\left([\cos(\theta_0 + \delta\theta_{e,far}) - \cos(\theta_0 + \delta\theta_{e,near})]\sigma_{s_z}\right)^2 \end{aligned} \quad (4)$$

η is the local incidence angle and Δt = 1 day for ERS-1&2 tandem mission. In the worst case, σ_{s_y} = 100 cm and σ_{s_z} = 8 cm, a maximum velocity

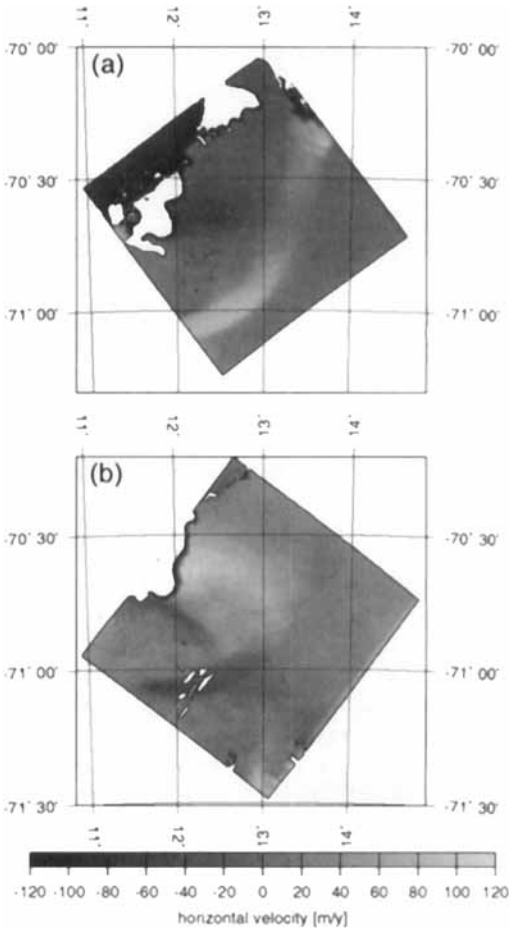

Fig. 6. Unwrapped and geocoded interferograms. (a) Frame 5715 of ascending track 316. (b) Frame 5085 of descending track 163. The grey values show relative ground range velocities of the ice surface towards (negative values) or off (positive values) the SAR sensor.

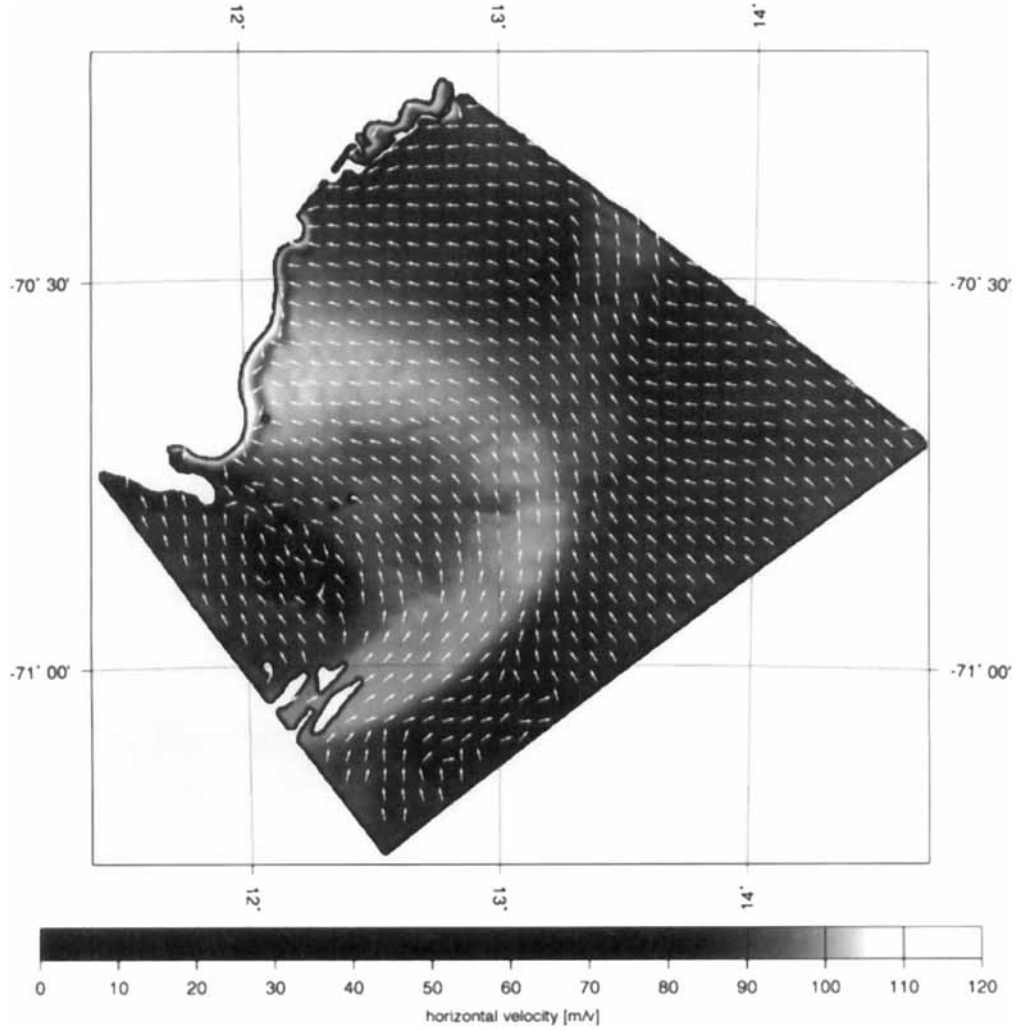

Fig. 7. Interferometrically derived ice velocities and directions.

error of about 159 m/y for SLCIs from near to far range or vice versa is possible, corresponding to a phase error of about $5.2 \times 2\pi$. A similar error estimation is given by Joughin et al. (1996).

Orbit errors are evident for the orbit couple 25354 and 5681 used to produce the interferogram for the ascending track (Fig. 5a). Residual fringes parallel to the along-track direction are clearly visible. To reduce velocity errors we estimated the interferometric baseline using four corner reflectors with known position, height and displacement rate. (The position of the corner reflectors can be seen in Fig. 1.) Because two of the four corner reflectors are situated outside frame 5715, the adjacent frame of track 316 covering these two reflectors (not shown in Fig. 1) was included in this computation step. The baseline estimation was carried out by fixing the vertical component B_z to the value calculated from precise ERS orbit products and by computing the horizontal component B_y depending on the along-track position. A similar approach has already been used by Zebker et al. (1994). The normal component B_n of the estimated baseline for the image center is about 7.8 m instead of about 9.0 m if using original precise ERS orbits.

To derive velocities phase unwrapping is necessary. Using the enhanced baseline the comparison of interferometrically derived slant

Table 2. Comparison of magnitude v and azimuth A of interferometrically derived velocity vectors with ground based observations. gt = ground truth; 1/2 = ERS-1&2.

Signal	v_{gt} [m/y]	$v_{1/2}$ [m/y]	$v_{gt}-v_{1/2}$ [m/y]	A_{gt} [°]	$A_{1/2}$ [°]	$A_{gt}-A_{1/2}$ [°]
U9	17.15	25.70	−8.55	326.40	322.19	4.21
U10	20.90	20.99	−0.09	335.50	327.08	8.42
U11	29.86	28.62	1.24	4.40	347.22	17.18
U13	80.84	83.81	−2.97	10.60	0.00	10.60
U14	58.03	56.93	1.10	348.70	335.12	13.58
U15	48.16	51.36	−3.20	338.20	328.12	10.08
U16	54.34	57.34	−3.00	342.10	336.05	6.05
U19	2.28	4.71	−2.43	337.90	149.04	171.14
COR4	2.27	5.31	−3.04	345.32	62.45	77.13

range displacements with ground truth data is shown in Table 1. The agreement of the ground truth data with the surface displacements determined by SAR interferometry is at the subcentimetre level.

To combine ascending and descending tracks a precise geocoding was performed using the four corner reflectors (Fig. 6). If nearly horizontal ice velocities are assumed, the two dimensional ice velocity field can be derived for the overlapping area of frame 5715 and frame 5085. Taking into account a mean surface slope of about 1.8% for the inland ice within the overlapping area, this assumption causes an error of about 4% in the velocity estimate. Figure 7 shows the magnitude of ice velocity (grey-scaled) and the direction of the movement (white arrows). The comparison between the ground truth and the interferometric velocity vectors is shown in Table 2. The remaining differences are presumably caused by errors of the DEM used to remove topography, the assumption of nearly horizontal ice velocities and possible residual orbit errors of the descending track.

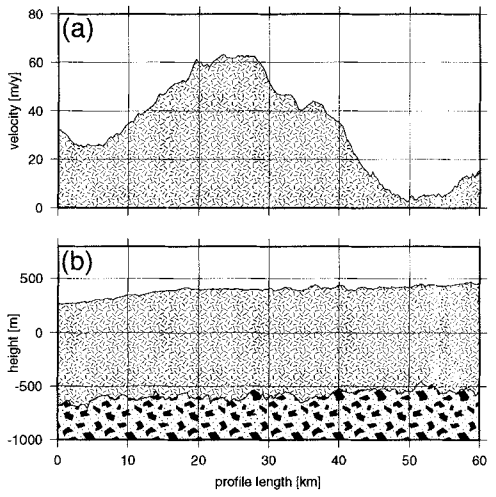

Fig. 8. Profile A. (a) Surface velocities perpendicular to the profile, derived interferometrically. (b) Surface and bedrock heights (Damm & Eisenburger 1996). For location of the profile see Fig. 1.

Conclusions and outlook

The gain of information when applying SAR interferometry is obvious. This shows the comparison of the obtained surface velocity field (Fig. 7) with the velocity vectors along surface traverses (Fig. 1). The more active ice stream and areas with smaller motions in the surrounding parts can easily be distinguished from each other. The high accuracy (cm level) of surface displacement determinations by SAR interferometry could be confirmed. Possible errors in motion estimates due to inaccuracy of precise ERS orbit products have to be emphasized.

The obtained surface velocities can be combined with radar ice thickness observations (see Fig. 8). Assuming that the mean velocity over a cross-section is within a few per cent of the mean surface velocity (Paterson 1994), the ice mass flux across a certain profile can be estimated. The demarcation of the ice stream within the inland ice using flow lines is rather difficult for the area under investigation. That may be one reason for the relatively high degree of error in the mass balance as obtained by the comparison of different cross-sections. Further investigations are planned to solve this problem. It should then also be possible to show too whether the ground-proved

decrease in surface heights by about 15 cm/y for the blue-ice area corresponds to a negative interferometrically derived mass balance.

The mass transport across the grounding line is of special interest. The location of the grounding line can be determined very easily by means of SAR interferometry considering the tidal displacement of the ice shelves (see e.g. Rignot 1996; Dietrich et al. 1998). As a next step of our investigations it is anticipated to determine reliable estimates of the mass flux across the grounding line.

Acknowledgements. – The authors would like to thank K. Shibuya and K. Doi, National Institute of Polar Research (NIPR), Tokyo, Japan, for their support in recording ERS-1&2 SAR tandem data at Syowa station. We thank R. Hartmann and W. Winzer (Jena-Optronik GmbH) for providing JENA-SAR. The extensive support of the Bundesanstalt für Geowissenschaften und Rohstoffe (BGR) Hannover during the expedition GeoMaud 1995/96 is gratefully acknowledged. This research was supported by Bundesministerium für Bildung und Forschung (BMBF) grants 03PL016B and 03PL013. SLCIs copyright by European Space Agency 1997.

References

Damm, V. & Eisenburger, D. 1996: *Bericht über hubschraubergestützte Radar-Eisdickenmessungen im zentralen Queen Maud Land während der Antarktisexpedition GeoMaud 1995/96. (Report on airborne ice thickness measurements with radio echo sounding in the central Dronning Maud Land during the Antarctic expedition GeoMaud 1995/96.) BGR Report no. 114890.* 13 pp. Hannover: Federal Institute for Geosciences and Natural Resources (BGR).

Dietrich, R. (ed.) 1996: *The Geodetic Antarctic Project GAP95 – German contributions to the SCAR 95 Epoch Campaign.* München: Deutsche Geodätische Kommission, Reihe B, Heft 304.

Dietrich, R., Dach, R., Korth, W., Metzig, R. & Perlt, J. 1998: Ice – ocean – solid earth interactions in Dronning Maud Land / Antarctica: a geodetic approach to solve open questions. In R. Forsberg, M. Feissel, & R. Dietrich (eds.): *Geodesy on the move, gravity, geoid, geodynamics, and Antarctica. Proceedings of the IAG Scientific Assembly.* Rio de Janeiro, 3–9 September 1997. *IAG Symposia. Vol. 119.* Pp. 504–509. Berlin: Springer.

Geudtner, D. 1995: *Die interferometrische Verarbeitung von SAR-Daten des ERS-1* (Interferometric processing of ERS-1 SAR-data). DLR-Forschungsbericht 95-28. Deutsche Forschungsanstalt für Luft- und Raumfahrt Köln.

Giovinetto, M. B., Waters, N. M. & Bentley, C. R. 1990: Depending of Antarctic surface mass balance on temperature, elevation, and distance to open ocean. *J. Geophys. Res. 95(D4),* 3517–3531.

Goldstein, R. M., Engelhardt, H., Kamb, B. & Frolich, R. M. 1993: Satellite radar interferometry for monitoring ice sheet motion: application to an Antarctic ice stream. *Science 262(5139),* 1525–1530.

Gruber, T., Massmann, F. H. & Reigber, C. 1996: *The German PAF for ERS, ERS D-PAF Altimeter and Orbit Global Products Manual.* ERS-D-GPM-31200. Potsdam: GeoForschungZentrum.

Joughin, I., Kwok, R. & Fahnestock, M. 1996: Estimation of ice-sheet motion using satellite radar interferometry: method and error analysis with application to Humboldt Glacier, Greenland. *J. Glaciol. 42(142),* 564–575.

Korth, W. & Dietrich, R. 1996: *Ergebnisse geodätischer Arbeiten im Gebiet der Schirmacheroase/Antarktika 1988–1993. (Results of geodetic field work in the region of the Schirmacheroase/Antarctica 1988–1993.)* München: Deutsche Geodätische Kommission, Reihe B, Heft 301.

Korth, W., Dietrich, R., Reitmayr, G. & Damm, V. 1998: Regional geoid improvement based on surface gravity data. In R. Forsberg, M. Feissel & R. Dietrich (eds.): *Geodesy on the move, gravity, geoid, geodynamics, and Antarctica. Proceedings of the IAG Scientific Assembly.* Rio de Janeiro, 3–9 September 1997. *IAG Symposia. Vol. 119.* Pp. 523–528. Berlin: Springer.

Korth, W., Perlt, J., Dach, R. & Dietrich, R. 1996: Repeated observations of ice surface heights near Schirmacher Oasis for ice mass balance studies. In R. Dietrich (ed.): *The Geodetic Antarctic Project GAP95 – German contributions to the SCAR 95 Epoch Campaign.* München: Deutsche Geodätische Kommission, Reihe B, Heft 304.

Massonnet, D., Rossi, M., Carmona, C., Adragna, F., Peltzer, G. & Rabaute, T. 1993: The displacement field of the Landers earthquake mapped by radar interferometry. *Nature 364(6433),* 138–142.

Paterson, W. S. B. 1994: *The physics of glaciers.* Third edition. Oxford: Pergamon Press.

Rignot, E. 1996: Tidal motion, ice velocity and melt rate of Petermann Gletscher, Greenland, measured from radar interferometry. *J. Glaciol. 42(142),* 476–485.

Scharroo, R. & Visser, P. 1998: A new gravity field model for the ERS missions. *Ann. Geophys. Society Symposia, Solid Earth, Geophysics & Geodesy 16(1),* C357.

Zebker, H. A., Werner, C. L., Rosen, P. A. & Hensley, S. 1994: Accuracy of topographic maps derived from ERS-1 interferometric radar. *IEEE Trans. Geosci. Rem. Sen. 42(4),* 823–836.